sustainability

MDPI

Article

Modeling and Evaluating Soil Salt and Water Transport in a Cultivated Land–Wasteland–Lake System of Hetao, Yellow River Basin's Upper Reaches

Guoshuai Wang [1,2], Bing Xu [1,2], Pengcheng Tang [1,2], Haibin Shi [3,*], Delong Tian [1,2], Chen Zhang [1,2], Jie Ren [1,2] and Zekun Li [1,2]

[1] Institute of Water Resources for Pastoral Area Ministry of Water Resources, Hohhot 010020, China
[2] Yinshanbeilu Grassland Eco-Hydrology National Observation and Research Station, China Institute of Water Resources and Hydropower Research, Beijing 100038, China
[3] College of Water Conservancy and Civil Engineering, Inner Mongolia Agricultural University, Hohhot 010018, China
* Correspondence: shb@imau.edu.cn; Tel.: +86-13500613853 or +86-04714300177

Abstract: With the implementation of water-conservation projects in the Hetao Irrigation District (HID), great changes have taken place in the ecohydrological process. A cultivated land–wasteland–lake system in the upper Yellow River Basin (YRB) was chosen to study the soil salt and water transport process with the Hydrus-1D model. The model parameters were calibrated and validated by measuring the soil salt and water data. Measured values were in good agreement with the simulated values. The results showed, in the whole growth period, the deep percolation of cultivated land was 34–40% of the total applied water (rainfall and irrigation). The capillary rise in the cultivated land, wasteland, and lake boundary was 24%, 29–35%, and 62–68% of their own evapotranspiration, respectively. The capillary rise in the lake boundary was about 2 times that of the wasteland and 2.6 times that of the cultivated land. The salt storage in the 1 m soil zone of the lake boundary was more than 10% and 18% greater than that of the wasteland and cultivated land, respectively. The salt of the capillary rise in the lake boundary exceeded that of the wasteland by a factor of three. The salt accumulation in the upper soil zone of the cultivated land, wasteland, and lake boundary was 13%, 37%, and 48%. Soil salinization in the upper soil zone of the wasteland and lake boundary was serious, and some measures should be taken to reduce the salt content to prevent soil salinization. The results act as a theoretical basis for the ecohydrological control of the HID.

Keywords: Hydrus-1D; different land types; water salt transport process; water balance; salt accumulation; distributed simulation

check for updates

Citation: Wang, G.; Xu, B.; Tang, P.; Shi, H.; Tian, D.; Zhang, C.; Ren, J.; Li, Z. Modeling and Evaluating Soil Salt and Water Transport in a Cultivated Land–Wasteland–Lake System of Hetao, Yellow River Basin's Upper Reaches. *Sustainability* **2022**, *14*, 14410. https://doi.org/10.3390/su142114410

Academic Editor: Asad Sarwar Qureshi

Received: 11 October 2022
Accepted: 31 October 2022
Published: 3 November 2022

Publisher's Note: MDPI stays neutral with regard to jurisdictional claims in published maps and institutional affiliations.

Copyright: © 2022 by the authors. Licensee MDPI, Basel, Switzerland. This article is an open access article distributed under the terms and conditions of the Creative Commons Attribution (CC BY) license (https://creativecommons.org/licenses/by/4.0/).

1. Introduction

Water deficits and soil salinization are the two major limitations on agricultural production and the ecological environment [1]. Irrigation water is seriously scarce in the semi-arid and arid areas of the world, and approximately one-fifth of irrigated agriculture is adversely affected by soil salinity [2]. Agricultural areas that are located in arid and semi-arid irrigation districts occupy the typical characteristics of shallow groundwater depth and fragmented land cover, for example, the Yellow River Basin (YRB) irrigation area, China [3], Central Asia's Fergana Valley [4], and India's Indo-Gangetic Plain [5], where the agro-hydrological cycles are extremely complex processes associated with soil water, salt migration, atmosphere, groundwater dynamics, and vegetation growth. Understanding these agro-hydrological processes is extremely significant for the efficient use of water resources and the control of salinization.

The Hetao Irrigation District (HID), in the upper reaches of the YRB, China, is a large salinized irrigation district. Due to poor irrigation and drainage practices, a large

volume of diverted water has been lost because of canal seeps, deep percolation, surface runoff, and evaporation, which has resulted in the low utilization of irrigation water, shallow groundwater depth, and soil salinization [5]. Water-conservation projects have been implemented in the HID to improve water conveyance since 2000 [6,7]. With the implementation of water-conservation projects, great changes have taken place in the soil, groundwater, and ecological environment of the irrigation district [8]. The regional water–salt balance system is out of balance, and as a result, many new problems have arisen in the ecological environment, such as the decline of the groundwater level, pollution in the soil and water environment, and a shrinking wetland and lake area [9]. Han et al. (2019) pointed out that lakes and wetlands are intricate systems in arid and semi-arid areas, in which moisture and salinity are continuously changing, and are especially sensitive to climate change and human activities [10]. At present, the amount of water diverted from the Yellow River to the HID is about 4.4–4.6 billion m^3, which transports large quantities of salt to the irrigation district. Wu et al. (2009) pointed out that about 70% of the salt could not be drained from the irrigation district [11]. How does salt transport occur in the irrigation district? This question has attracted the attention of many scholars, and a large amount of research has been published on salt and water transport in the HID.

Qi et al. (2018) revealed that complete film mulch treatments showed clear desalination impacts, whereas partial film mulch modes resulted in secondary salinization in the 0–40 cm soil zone [12]. Ren et al. (2016) used the HYDRUS-dualKc coupling model to simulate soil salt and water transport characteristics under different vegetation covers and pointed out that the wasteland contained nearly 50% of the salt introduced by irrigation [5]. Zhu et al. (2013) reconstructed a three-dimensional saturated–unsaturated solute transport model (WSMS-Q3D) to evaluate groundwater transport in the Yonglian Irrigation District (YID) of the HID [13]. Mao et al. (2017) proposed that the salt in the aquifer is transported from the canal irrigation area to the well irrigation area by using the SALTMOD model [14]. Xu et al. (2012) studied the water–salt dynamic between groundwater and soil in the YID using the SWAP-MODFLOW coupling model [15]. Ren et al. (2016) demonstrated the large impact of lateral groundwater exchange between different fields on the transport of groundwater and soil water, salts, nutrients, and vegetation growth [5]. Wu et al. (2009) showed that leached salts and surplus water are transported to relatively low-elevation, unirrigated natural lands from irrigated croplands. This process alleviated soil salinity in farmland and increased soil salinization in natural areas [11]. Ren et al. (2019) analyzed the spatiotemporal characteristics of soil salinity on three scales: regional, canal, and field. Their results indicated that: (1) the distribution of soil salinity on the regional scale was dominated by the depth of groundwater and topography; (2) canal-scale soil salinity was dominated by the patterns of cropping and irrigation; (3) field-scale salinity was dominated by the uniformity of field irrigation and micro-topography [16]. Li et al. (2010) used the Hydrus-1D model to simulate salt and water transport in wastelands and revealed that soil salt in the 5 cm and 10 cm soil zones increased by 66.10% and 63.89%, respectively [17]. The above studies investigated salt and water redistribution on the field scale and regional scale in the HID. Wasteland is distributed in the gaps of cultivated land and is surrounded by lakes. Cultivated land, wastelands, and adjacent lakes are the typical distribution forms in the HID. However, there have been few studies on salt and water redistribution in the saturated–unsaturated zone of the soil profile of a cultivated land–wasteland–lake system.

Mathematical models are an effective approach to investigating the movement of soil salt and water. Kanzari et al. (2018) studied water flow and salt transport using the Hydrus-1D model in a semi-arid region in Tunisia [18]. Bashir et al. (2018) used the Hydrus-1D model to investigate the impact of soil texture and climate on the dynamics of soil salt and water in variably saturated soils [19]. Dong et al. (2019) predicted the impact of long-term irrigation on groundwater quality using Hydrus-1D in the Kongque River region [20]. Wu et al. (2019) applied the Hydrus-1D model to study soil salinity due to seepage from a lowland reservoir in Xinjiang Province, China [21]. Slama et al. (2019) studied the effect of climate change and rainfall structure on groundwater and soil salinization using the

Hydrus-1D model in the semi-arid coastal plain of Korba in Tunisia [22]. Liu et al. (2019) applied the Hydrus-1D model to evaluate soil salt transport in wheat–maize cultivated lands with different texture layers in the lowland of the North China Plain [23]. However, the Hydrus-1D model has rarely been used to evaluate and analyze the internal relationship between salt and water dynamics in a cultivated land–wasteland–lake system in the HID.

Therefore, the primary aims of this study were to: (1) understand the mechanism of soil water consumption and salt accumulation; (2) reveal the relationship between soil salt and water in a cultivated land–wasteland–lake system; and (3) use the Hydrus-1D model, calibrated by field observation data, to evaluate the soil salt and water balance and quantitatively estimate the soil salt and water in the typical period. The results of this study provide a theoretical basis for the effective utilization of water resources and soil salinization control in the HID.

2. Study Area, Methods, and Materials

2.1. The Study Area

The HID is approximately 50 km long from north to south and 250 km wide from east to west (Figure 1). The HID extends over 1.12 Mha; the cultivated land area is 5.74×10^5 hm^2, the wasteland area is 2.10×10^5 hm^2, and the water area is 1.30×10^4 hm^2 [5,24]. Wasteland and lakes are distributed in patches, and the formation of lakes mainly depends on the irrigation water. A large amount of salt has accumulated in the low-lying wetland [9]. Ground slope is from 1/5000 to 1/8000 from the west to the east and from 1/4000 to 1/8000 from the south to the north. The depth of groundwater varies between 0.5 and 3 m over the whole year [25]. Hetao has the characteristics of a continental arid and semi-arid climate. Annual precipitation is about 50–144.2 mm. The rainy season extends from June to August, accounting for 70% of annual precipitation. The study area has a mean annual temperature of 7.5 °C and the average annual evaporation is 2237 mm. Maize and sunflower are the main crops in Hetao.

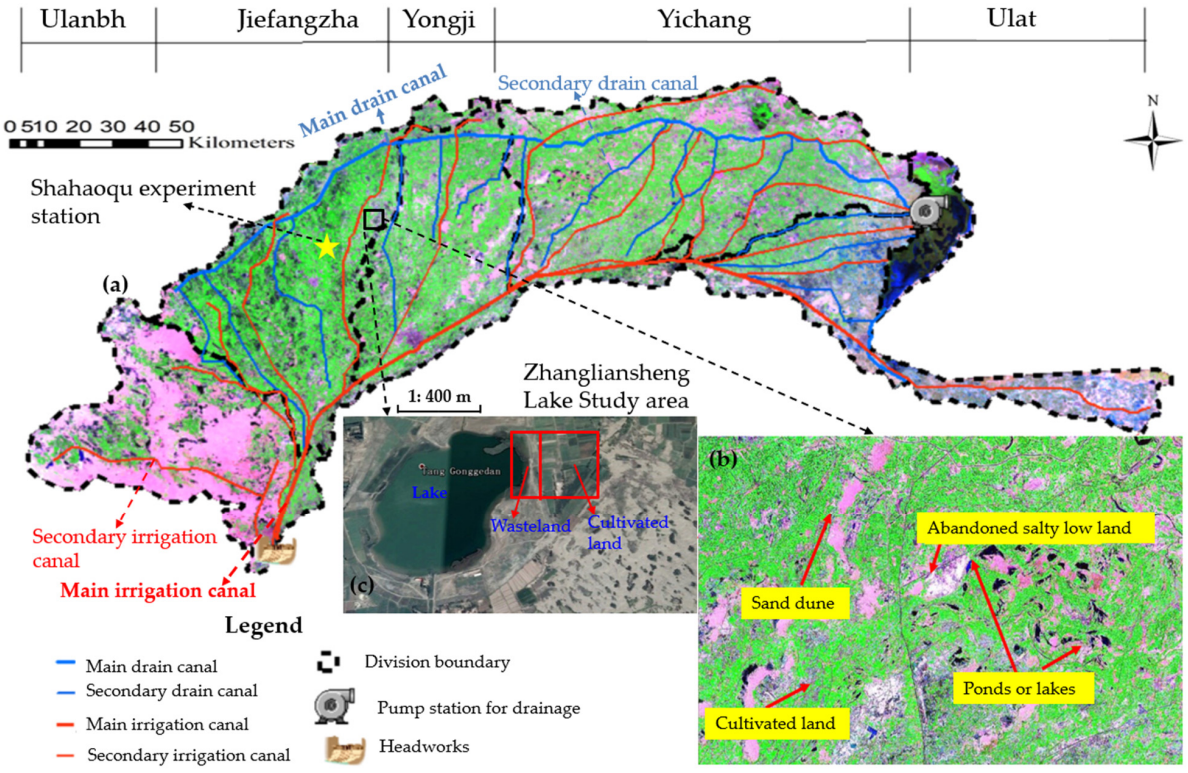

Figure 1. Hetao Irrigation District with representations of: (**a**) the dominant irrigation drainage canals and (**b**) the cultivated land in green. Sand dunes in purple; ponds or lakes in blue; abandoned salty lowlands in white. (**c**) study area in red [26].

The study area is located at the Zhangliansheng site (40°54′36″ N, 107°15′59″ E), which is east of the Jiefangzha Irrigation District (JID) in Hetao (Figure 1). The areas of the cultivated land, wasteland, and lake are 3.7×10^4 m^2, 4.4×10^4 m^2, and 5.12×10^5 m^2, respectively (Figure 2). The results of a real-time kinematic (RTK) showed that the maximum ground height difference in the farmland was 15 cm, and the average height of the farmland was 45 cm higher than that of the wasteland. The changes in the groundwater depth during the crop growth period were 50–220 cm for the cultivated land, 70–160 cm for the wasteland, and 30–140 cm for the lake boundary. The main crop in the study area is sunflower. The soil texture of the 300 cm soil zone in the study area is mainly sand and sandy loam (Table 1).

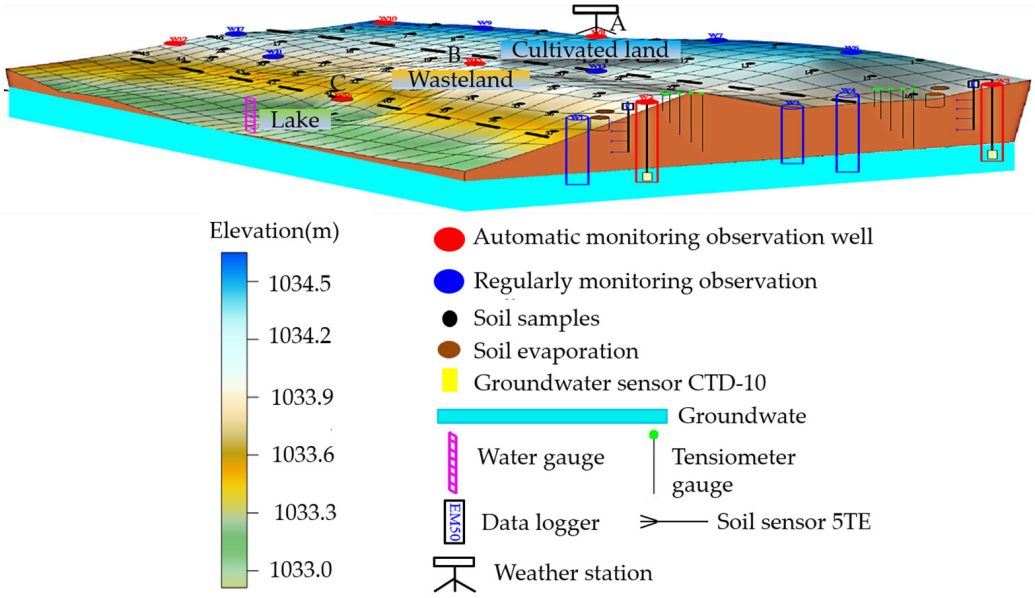

Figure 2. Experimental layout of the study area.

Table 1. Physical characteristics of the soil in the study area.

Site	Depth of Soil (cm)	The Distribution of Soil Particle Sizes (%)			Bulk Soil Density (g cm^{-3})	K_s (Saturated Hydraulic Conductivity) (cm d^{-1})	θ_s (Saturated Water Content) (cm^3 cm^{-3})
		Clay (<0.02 mm)	Silt (0.02~0.5 mm)	Sand (0.5~2 mm)			
A	0~300	3.16	45.28	51.56	1.51	19.67	0.31
B	0~80	2.18	42.65	55.17	1.53	22.10	0.36
	80~300	2.49	7.68	89.83	1.61	230.84	0.33
C	0~20	5.61	14.32	80.06	1.52	197.76	0.38
	20~300	0.42	5.88	94.12	1.62	315.12	0.31

2.2. Data Observation and Collection

2.2.1. Meteorological Data

The daily meteorological data, including temperature, relative humidity, sunshine duration, wind speed, and rainfall, were collected. Based on the daily meteorological data and the Penman–Monteith equation, the daily reference evapotranspiration (ET_0) was calculated [27]. The ET_0 and rainfall in 2018 and 2019 are shown in Figure 3. The precipitation in 2018 and 2019 was 124 mm and 78 mm, respectively. The precipitation in the crop growth period (1 June to 1 October) was 109.6 mm and 64.88 mm (Figure 3). The average annual daily evapotranspiration was 2.7 mm/d. In the crop growth period, the average daily evapotranspiration was from 4.3 mm/d to 4.6 mm/d.

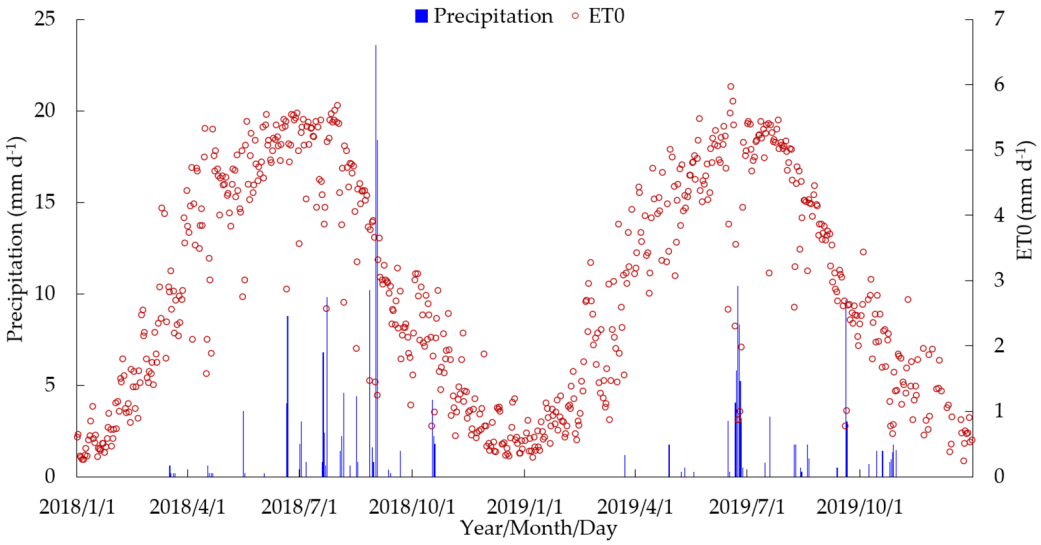

Figure 3. Precipitation and ET_0 (reference evapotranspiration) in 2018 and 2019.

2.2.2. Groundwater Data

Seventeen groundwater observation wells were established in the study area, including seven key observation wells (in red circle) and ten regularly observed wells (in blue circle). Automatic groundwater sensors (CTD-10, Meter Company, San Francisco, CA, USA) were installed in key observation wells, and an EM50 logger (Meter Company) was used to record groundwater table, temperature, and electrical conductivity (EC) data in one-hour intervals. The groundwater depth of the regularly observed wells was measured every 7 days. Three key observation wells, A (cultivated land), B (wasteland), and C (lake boundary), were selected to reveal groundwater dynamics (Figure 4). Figure 4 shows the dynamic process of groundwater depth during the growth period. The dynamics of the groundwater table were greatly affected by irrigation and rainfall.

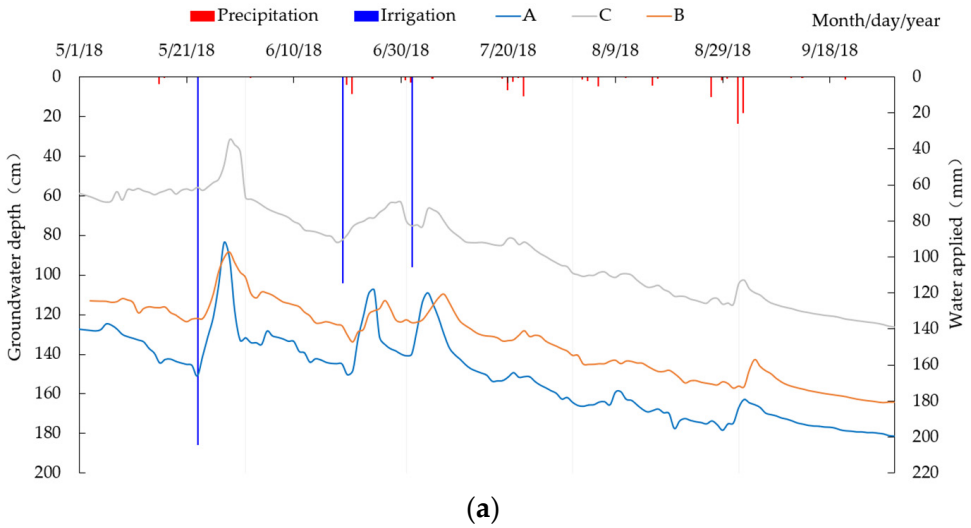

(**a**)

Figure 4. *Cont.*

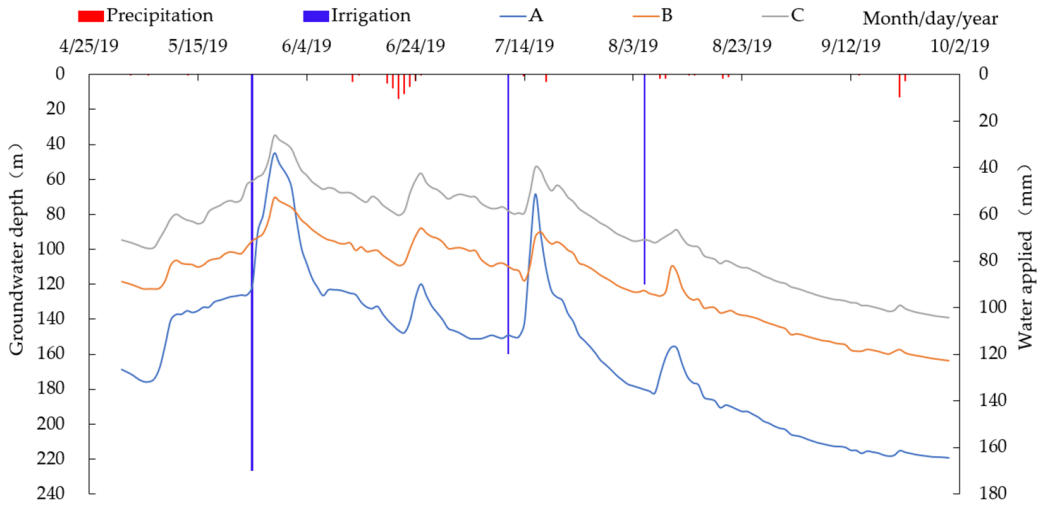

(**b**)

Figure 4. Groundwater table dynamics of three typical observation wells. Note: (**a**) Groundwater table dynamics at the site of A, B, C in 2018; (**b**) Groundwater table dynamics at the site of A, B, C in 2019.

2.2.3. Soil Data

There were 63 soil observation points in the study area. The distance between each soil observation point was 50 m. Soil samples in each soil zone (0 to 10, 10 to 20, 20 to 40, 40 to 60, 60 to 80, and 80 to 100 cm) were collected in 10-day intervals over the period of crop growing. The oven-drying method was used to measure soil moisture, and the EC values of the soil extract solution with a soil–water ratio of 1:5 was determined using a conductivity meter (DDS-307A type, Shanghai Youke Instrument Company, Shanghai, China). In addition, there were seven key soil observation points. The soil samples at the key soil observation points were collected in each soil zone (0–20, 20–40, 40–60, 60–80, 80–100, 100–120, 120–160, 60–200, 200–250, and 250–300 cm). Soil automatic sensors (5TE, Meter Company) were installed at the key observation points to monitor soil moisture, EC, and temperature, which were recorded by the EM50 logger.

The conversion formula of the *EC* measured by the 5TE in the *EC* values of the soil extract solution with a soil–water ratio of 1:5 is [28]:

$$EC_{1:5} = \frac{EC_{5TE} - 0.1505}{0.9595} \ (r = 0.975,\ p < 0.05,\ n = 96) \quad (1)$$

where $EC_{1:5}$ represents the *EC* values of the soil extract solution with a soil–water ratio of 1:5 (dS m^{-1}) and EC_{5TE} is the *EC* values measured by 5TE (dS m^{-1}).

The EC_e of all the samples was estimated using Equation (2) [29]:

$$EC_e = 5.88 \times EC_{1:5} + 1.33 \quad (2)$$

The conversion formula of $EC_{1:5}$ in soil salt (*SSC*) is [29]:

$$SSC = EC_{1:5} \times 3.7657 - 0.2405 \quad (3)$$

where *SSC* is soil salt (g kg^{-1}).

Salt in the soil solution (C_{SW}) can be calculated as [30]:

$$C_{SW} = \frac{SSC \cdot \gamma}{\theta} \quad (4)$$

where θ is the moisture of the soil (cm^3 cm^{-3}), γ indicates dry soil bulk density (g cm^{-3}), and C_{sw} is salt in the soil solution (g L^{-1}).

Three key soil points, A (cultivated land), B (wasteland), and C (lake boundary), were selected to unveil soil textural properties. The soil particle sizes were measured utilizing a dry particle size analyzer (Helos & Rodos, Germany New Partec, Dresden, Germany). The saturated hydraulic conductivity, bulk density, and saturated moisture of undisturbed soil samples were measured (100 m^3). The results showed that the soil texture in the 0–300 cm soil zone of cultivated land was sandy loam. The soil profile of the wasteland and lake boundary could be described by two layers. The soil texture in the 0–80 cm soil zone of the wasteland was sandy loam, and it was sand in the 80–300 cm soil zone. The soil texture in the 0–20 cm soil zone of the lake boundary was sandy loam, and in the 20–300 cm soil zone, it was sand. Table 1 summarizes the important physical properties of soil at a depth of 0–300 cm in the cultivated land (A), wasteland (B), and lake boundary (C).

2.2.4. Water Sample Data

Table 2 presents the irrigation schedule for 2018 and 2019. The scheduling of irrigation depends on both the experience of farmers and the conditions of canal water. A trapezoidal thin-wall weir was used to measure the irrigation volumes. Three irrigation events were conducted per year. Rainfall and irrigation water were collected on rainy days and during the irrigation period. The lake and groundwater samples were collected every 10 days. Each water sample was collected in triplicate. The *EC* (Electrical Conductivity) was measured using a conductivity meter (DDS-307A). The conversion formula of the *EC* and the total dissolved solids (*TDS*) is [31]:

$$TDS\ (g/L) = 0.69EC_w\ (dS/m) \quad (5)$$

Table 2. Irrigation scheduling in 2018 and 2019.

Crop	Irrigation Events	Irrigation Depth (mm)	TDS (Total Dissolved Solids) (g/L)
Sunflower	23 May 2018	186	0.59
	23 June 2018	104	0.53
	4 July 2018	96	0.61
Sunflower	29 May 2019	170	0.56
	13 July 2019	120	0.65
	6 August 2019	90	0.61

The irrigation schedule of the study area is shown in Table 2. The irrigation quota was 386 mm and 380 mm in 2018 and 2019. The *TDS* of irrigation water varied between 0.54 g/L and 0.65 g/L.

2.2.5. Crop Growth Period

The sunflower development stages were recorded (Table 3). The planting time in 2018 and 2019 was 31 May and 2 June, respectively. It took 113 days and 111 days from sowing to maturity in 2018 and 2019.

Table 3. Stages of crop growth over two years of experiments (2018 and 2019).

Year	Crop	Date of Planting	Stage of Growth				Total
			Initial	Development	Middle Season	Late Season	
2018	Sunflower	31 May	25	30	38	20	113
2019	Sunflower	2 June	25	30	35	21	111

2.3. Soil Salt and Water Dynamic Model

Hydrus-1D is a vertical, one-dimensional model that is used to simulate soil water flow, heat and solute transport, and root water uptake in a saturated–unsaturated soil

profile [32]. With the improvement of the Hydrus-1D model, it has been widely applied to simulate carbon dioxide and major ion solution movement.

2.3.1. The Equation for Soil Water Flow

The governing equation for soil water flow is a modified form of the Richards equation:

$$\frac{\partial \theta}{\partial t} = \frac{\partial}{\partial z}\left[K(\frac{\partial h}{\partial z} + 1)\right] - S \tag{6}$$

where θ is the water volumetric content ($cm^3\ cm^{-3}$), z represents the vertical space coordinate (cm) (positive upward), t is time (d), h is the water pressure head (cm), K is the function of hydraulic conductivity ($cm\ d^{-1}$), and S represents a sink term ($cm^3\ cm^{-3}\ d^{-1}$) representing the rate of water uptake by roots.

The hydraulic properties of soil are represented by the van Genuchten and Mualem [33,34] model:

$$S_e(h) = \frac{\theta(h) - \theta_r}{\theta_s - \theta_r} = (1 + \alpha|h|^n)^{-m} \tag{7}$$

$$K(h) = K_s S_e^{\ell}\left[1 - (1 - S_e^{1/m})^m\right]^2 \tag{8}$$

where S_e represents effective saturation (−), θ_r is the residual moisture ($cm^3\ cm^{-3}$), θ_s is the saturated moisture ($cm^3\ cm^{-3}$), K_s is hydraulic conductivity under a saturated condition ($cm\ day^{-1}$), α (cm^{-1}), n (−) and m (−) are statistical parameters, and l is the pore connectivity parameter (−).

The impacts of osmotic and water stress on the uptake of water by roots are taken to be multiplicative:

$$S(h, h_\phi, z) = \alpha_{rw}(h)\alpha_{rs}(h_\phi)b(z)T_p \tag{9}$$

where T_p is the plausible rate of the uptake of water ($cm\ d^{-1}$), h_ϕ represents the osmotic head (cm), $b(z)$ is the distribution of the normalized uptake of water in the root zone (cm^{-1}), and $\alpha_{rs}(h_\phi)$ and $\alpha_{rw}(h)$ are osmotic response and water stress response functions, respectively. The present study selected the function form of Feddes to estimate $\alpha_{rw}(h)$ [35] and the modified S-shape function [36] by Homaee et al. (2002) and Dirksen et al. (1988) to estimate $\alpha_{rs}(h_\phi)$ [37,38].

2.3.2. The Equation for Soil Solute Transport

Solute transport was described using the convective–dispersive equation:

$$\frac{\partial(\theta c + \rho_b S)}{\partial t} = -\frac{\partial(qc)}{\partial z} + \frac{\partial}{\partial z}\left[\theta(D_{dif} + D_{dis})\frac{\partial c}{\partial z}\right] \tag{10}$$

where ρ_b is bulk soil density ($g\ cm^{-3}$), c is the solute concentration of the liquid phase ($mg\ cm^{-3}$ or $g\ L^{-1}$), s is the concentration of the adsorbent ($g\ g^{-1}$), q represents the water vertical flux ($cm\ d^{-1}$), D_{dif} represents the coefficient of diffusion ($cm^2\ d^{-1}$), and D_{dis} represents the coefficient of dispersion ($cm^2\ d^{-1}$).

2.3.3. Evaporation and Transpiration

The potential evapotranspiration of crops (ET_p) was estimated as $ET_p = K_c \times ET_0$, where K_c is the sunflower crop coefficient. The K_c values of sunflower were 0.35, 1.15, and 0.35 for the late, middle, and early growth stages, respectively, according to FAO56 recommendations [27]. In the Hydrus-1D model, ET_P is categorized into potential transpiration (T_P) and potential soil evaporation (E_P) according to the leaf area index (LAI) [39,40].

$$T_P = ET_p(1 - e^{KLAI}) \tag{11}$$

$$E_P = ET_p - T_p \tag{12}$$

where K represents the coefficient of the extinction of the crop canopy—K was set to 0.83 in this study—and LAI represents the leaf area index.

2.4. Model Setup, Calibration, and Verification

2.4.1. Profile Discretization

Three key observation points, A (cultivated land), B (wasteland), and C (lake boundary), were selected to simulate the salt and water transport of soil profiles. The soil profiles of the cultivated land, wasteland, and lake boundary were each set as 300 cm below the surface. The soil profiles of the cultivated land, wasteland, and lake boundary were divided into one horizon, two horizons, and two horizons, respectively, as per the texture of soil shown in Table 1. The 1D, vertical profile of the soil was subdivided into 301 nodes with 1 cm uniform spacing. The period of 1 June to 30 September was chosen as the period of simulation. The initial timestep, minimum timestep, and maximum timestep were 0.1 d, 0.001 d, and 5 d, respectively. The simulation timesteps and simulation domain were the same for the cultivated land, wasteland, and lake boundary.

2.4.2. Initial Condition and Boundary Condition

The atmosphere boundary condition containing the surface layer was set to the upper water flow boundary condition, and the variable pressure head was assigned as the bottom boundary condition. The atmospheric boundary conditions need the daily rainfall and irrigation flux (cultivated land), potential evaporation, and transpiration data. The groundwater depth (GWD) needed to be measured, and it was then input into the time-variable settings of the pressure head of the bottom boundary condition.

The upper and bottom boundary conditions were set as the concentration flux boundary. The upper boundary condition of the cultivated land was the irrigation water concentration, and for the wasteland and lake boundary, it was the rainfall concentration (the default value of 0). The bottom boundary condition for the cultivated land, wasteland, and lake boundary was the groundwater concentration. The soil salt and water initial conditions were established according to field observation values.

A classical logistic growth function was used to model root growth. The present study assumed that a 50% rooting depth would be reached by halfway through the growing season [32]. According to field observations, the maximum depth of the roots of sunflower was set at 60 cm. The piecewise linear water stress function proposed by Feddes et al. (1978) [35] and the S-shaped salt stress function proposed by van Genuchten et al. (1984) [36] were used to analyze the effect of soil salt and water dynamics on crop root water uptake.

2.4.3. Model Parameters

The initial soil hydraulic parameters (θ_s, θ_r, α, n, K_s, and l) were determined according to the measured dry soil bulk density and the proportions of silt, clay, and sand, as well as soil water-retention data using Rosetta pedotransfer functions. The parameter for the transport of solutes (dispersivity length, L) was obtained according to prior studies [5,30,41]. The initial values of root water uptake (h_1, h_2, h_{3h}, h_{3l}, h_4, h_ϕ, and $h_{\phi 50}$) were taken from Hydrus-1D database and prior studies [5,30,41].

2.4.4. Calibration and Verification Procedures

The measured soil water and EC values in different layers of soil (i.e., 0 to 10, 10 to 20, 20 to 40, 40 to 60, 60 to 80, and 80 to 100 cm) relative to 2018 and 2019 were utilized to calibrate and verify the model, respectively. The regression coefficient (b), determination coefficient (R^2), mean relative error (MRE), and root mean square error (RMSE) were utilized to assess the performance of the model [30]:

$$RMSE = \sqrt{\frac{1}{N}\sum_{i-1}^{N}(P_i - O_i)^2} \quad (13)$$

$$R^2 = \left[\frac{\sum_{i=1}^{N} (O_i - \overline{O})(P_i - \overline{P})}{\left[\sum_{i=1}^{N} (O_i - \overline{O})^2\right]^{0.5} \left[\sum_{i=1}^{N} (P_i - \overline{P})^2\right]^{0.5}} \right]^2 \quad (14)$$

$$b = \frac{\sum_{i=1}^{N} O_i \times P_i}{\sum_{i=1}^{N} O_i^2} \quad (15)$$

$$MRE = \frac{1}{N} \sum_{i=1}^{N} \frac{(P_i - O_i)}{O_i} \times 100\% \quad (16)$$

where P_i and O_i represent the model-simulated and -measured values, respectively (i = 1, 2, . . . , N), N represents the observation number, and $\overline{P}$ and $\overline{O}$ are the means of the model simulations and measurements, respectively. Values of b approaching 1 and $RMSE$ and MRE near 0 indicate the good performance of the model. A value of R^2 near 1 indicates that the model performs well in representing the variation in the observed values.

2.4.5. Research Process

Based on the collected soil, groundwater, meteorological, crop growth, and irrigation data, this research studied the water and salt transport of the cultivated land, wasteland, and lake boundary with the Hydrus-1D model. The study flowchart was shown in Figure 5.

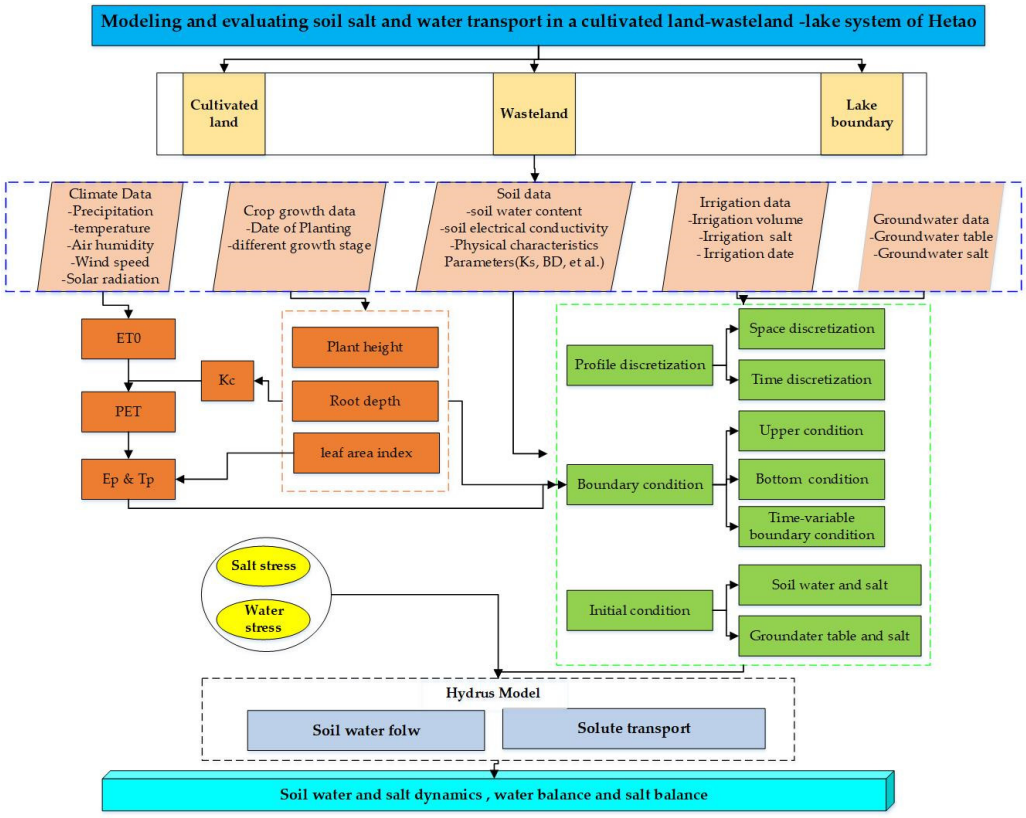

Figure 5. Study flowchart. Note: ET_0—reference crop evapotranspiration (cm d^{-1}); ET_p—potential evapotranspiration (cm d^{-1}), E_p—potential evaporation (cm d^{-1}); T_p—potential transpiration (cm d^{-1}), K_c—crop coefficient.

3. Results

3.1. Model Calibration

The model was calibrated using the experimental data from 2018. The simulated and measured values of the soil water content and EC in the different soil layers of the cultivated land, wasteland, and lake boundary are shown in Figures 6–8. The simulated

values of the soil water content were consistent with the measured values. The *MRE* values of the cultivated land, wasteland, and lake boundary varied from −0.43% to 4.89%, the *RMSE* values varied from 0.01 to 0.06 cm^3 cm^{-3}, the R^2 values varied from 0.75 to 0.90, and the b values were about 1 (Table 4). The salt transport processes were more complex than that of water; therefore, the simulated salt transport discrepancy was larger, especially in the 0–40 cm soil zone. Owing to the effects of rainfall, irrigation, and evaporation, the convective–dispersive process of salt transport was more complex and difficult to capture. The simulated salt transport discrepancies of the wasteland and the lake boundary, which were only affected by rainfall and evaporation, were smaller than those of the cultivated land. The simulated soil salt dynamics were also well-matched with observations. The *MRE* values of the cultivated land, wasteland, and lake boundary varied from −2.23% to −0.91%, the *RMSE* values were about 0.09 dS/m, the R^2 values varied from 0.89 to 0.91, and the *b* values varied from 0.95 to 0.97 (Table 4). The performance of the model in representing the soil salt and water transport processes was acceptable. Table 5 summarizes the values of the calibrated parameters representing soil hydraulic and solute transport processes, and Table 6 shows the root water uptake parameters.

Table 4. Values obtained for model goodness-of-fit statistics for calibration and verification.

Items	Site	Items	R^2	b	RMSE (cm^3 cm^{-3} or g L^{-1})	MRE (%)
Calibration (2018)	A	Soil water content	0.75	1.0	0.06	4.89
		Soil salinity concentration	0.89	0.95	0.08	−0.91
	B	Soil water content	0.88	1.02	0.02	−0.43
		Soil salinity concentration	0.90	0.96	0.09	−2.23
	C	Soil water content	0.90	0.9	0.01	0.15
		Soil salinity concentration	0.91	0.97	0.091	−1.26
Verification (2019)	A	Soil water content	0.92	1.0	0.01	−0.31
		Soil salinity concentration	0.56	1.0	0.15	4.43
	B	Soil water content	0.90	0.99	0.02	−0.92
		Soil salinity concentration	0.88	0.98	0.16	−0.013
	C	Soil water content	0.91	1.01	0.04	0.63
		Soil salinity concentration	0.89	1.02	0.34	−0.89

Table 5. Values assigned to the van parameters of the Genuchten–Mualem model and lengths of dispersion among different soil zones.

Site	Depths (cm)	Residual Soil Content θ_r (cm^3 cm^{-3})	Saturated Soil Content θ_s (cm^3 cm^{-3})	Shape Parameter α(-)	Empirical Parameter n (-)	Saturated Hydraulic Conductivity/K_s (cm d^{-1})	Molecular Diffusion Coefficient l (-)	Dispersion Coefficient L (cm)
A					Starting values			
	0~200	0.0271	0.312	0.035	1.12	19.67	0.7	20
					Calibrated values			
	0~200	0.0421	0.3911	0.006	8.11	21.12	3.0	15
B					Starting values			
	0~80	0.0262	0.36	0.043	1.12	22.1	0.7	20
	80~200	0.0442	0.33	0.038	2.05	230.84	1.0	10
					Calibrated values			
	0~80	0.0412	0.52	0.044	1.74	22.1	2.0	20
	80~200	0.0521	0.51	0.032	1.82	230.84	2.0	20
C					Starting values			
	0~20	0.0422	0.38	0.043	1.79	198.12	0.7	20
	20~200	0.0351	0.31	0.036	3.19	315.57	1	10
					Calibrated values			
	0~80	0.0422	0.41	0.042	1.51	25	0.5	15
	80~200	0.0351	0.39	0.036	1.23	242	0.5	25

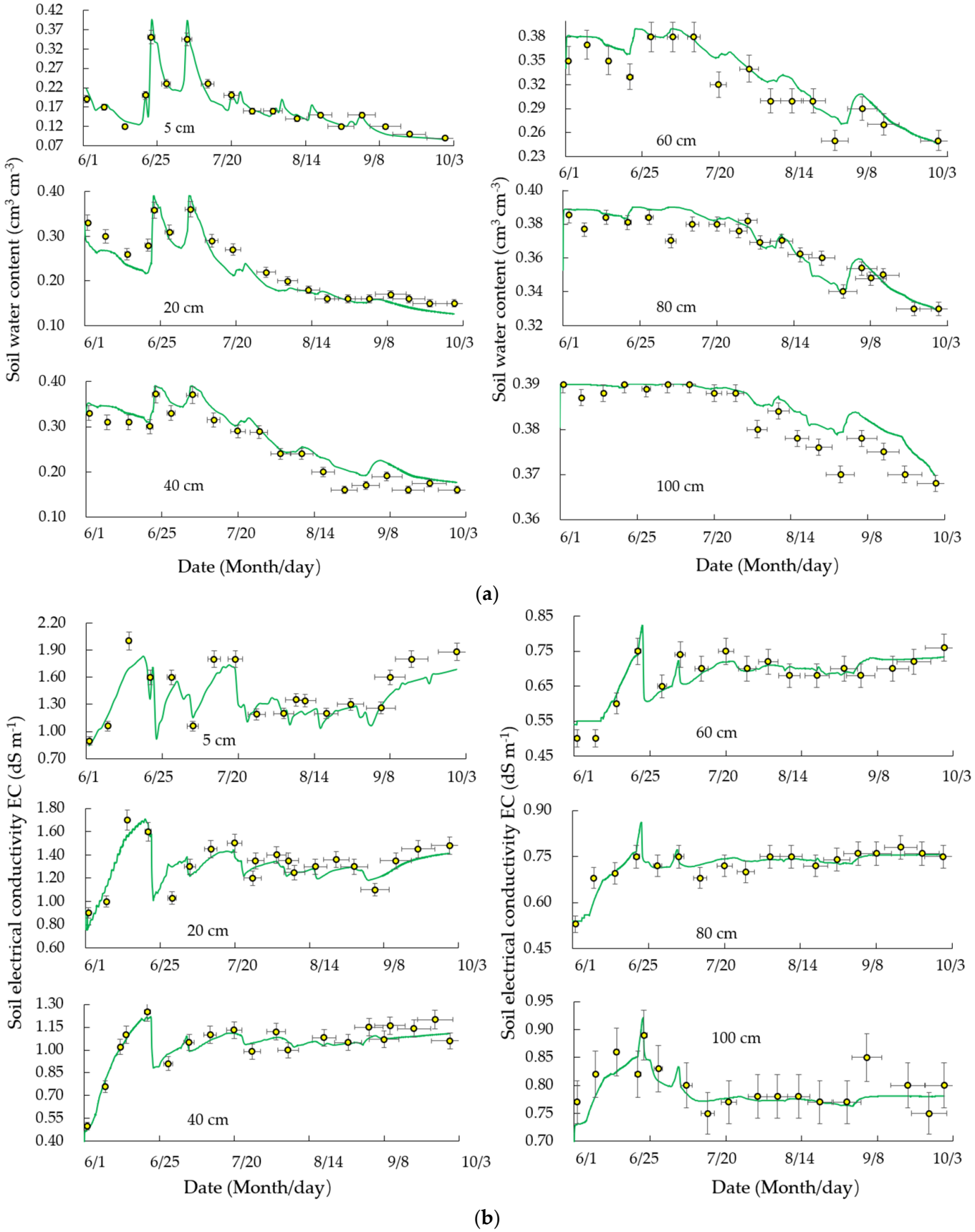

Figure 6. Model simulations (—) versus observed (·) soil water content (**a**) and soil electrical conductivity (**b**) for different layers of soil during the calibration of the model for the cultivated land.

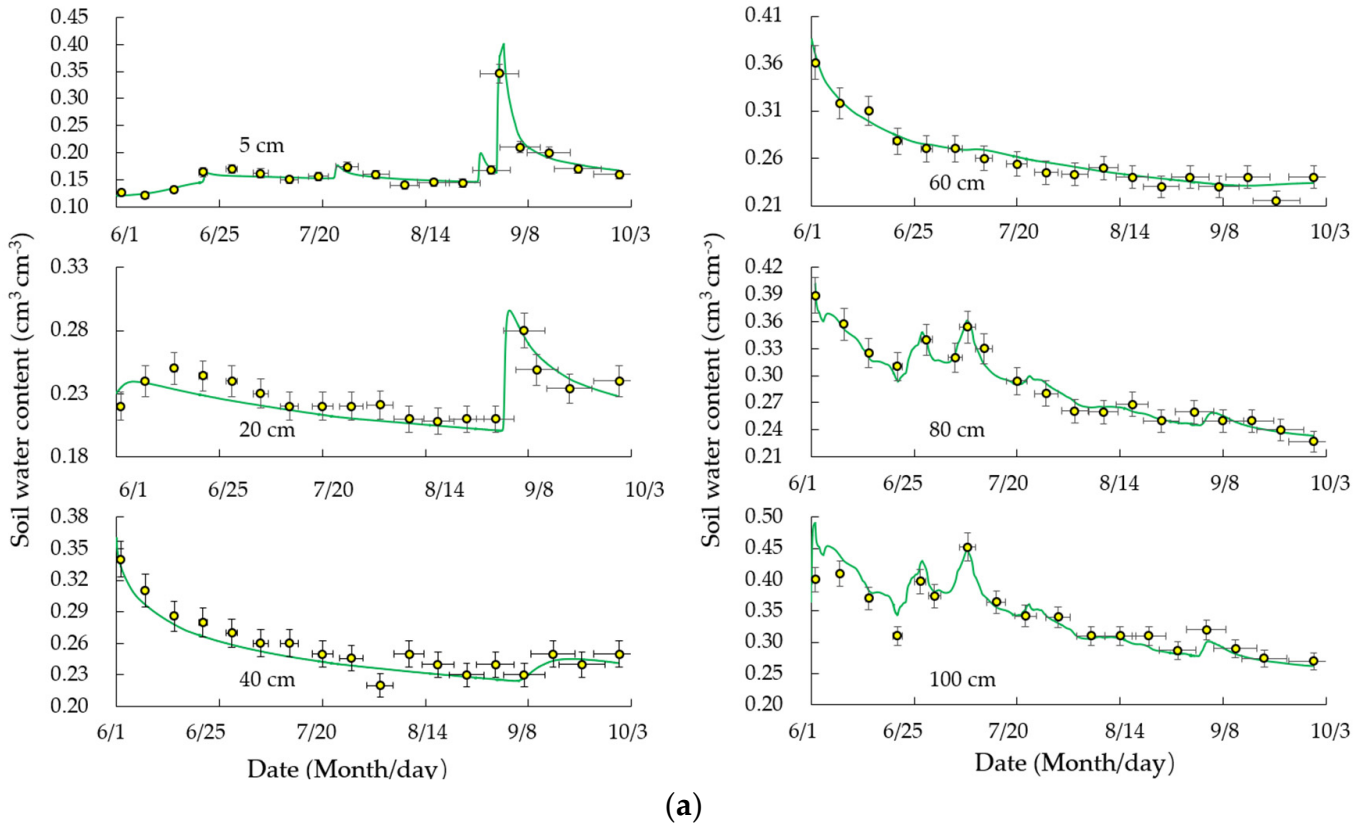

(**a**)

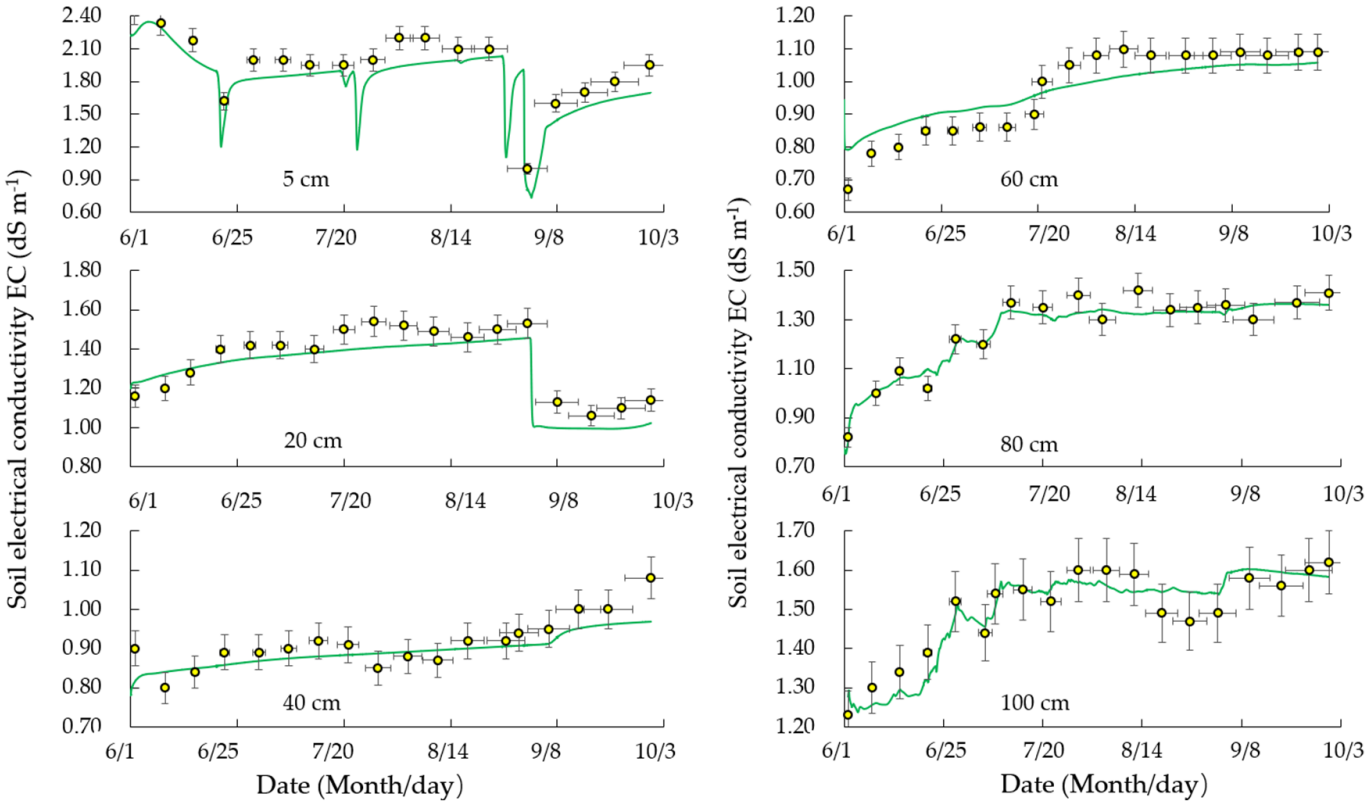

(**b**)

Figure 7. Model simulations (−) versus observed (·) soil water content (**a**) and soil electrical conductivity (**b**) for different layers of soil during the calibration of the model for the wasteland.

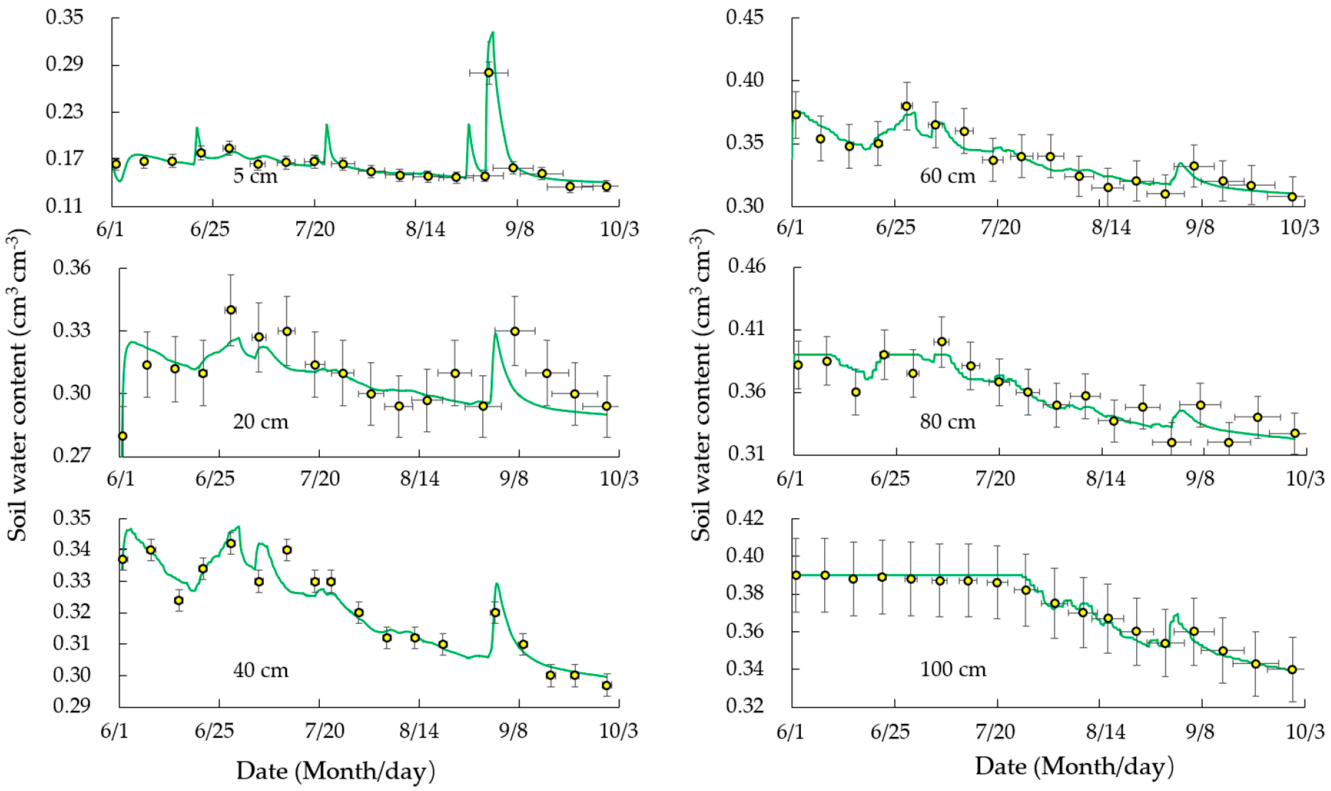

(**a**)

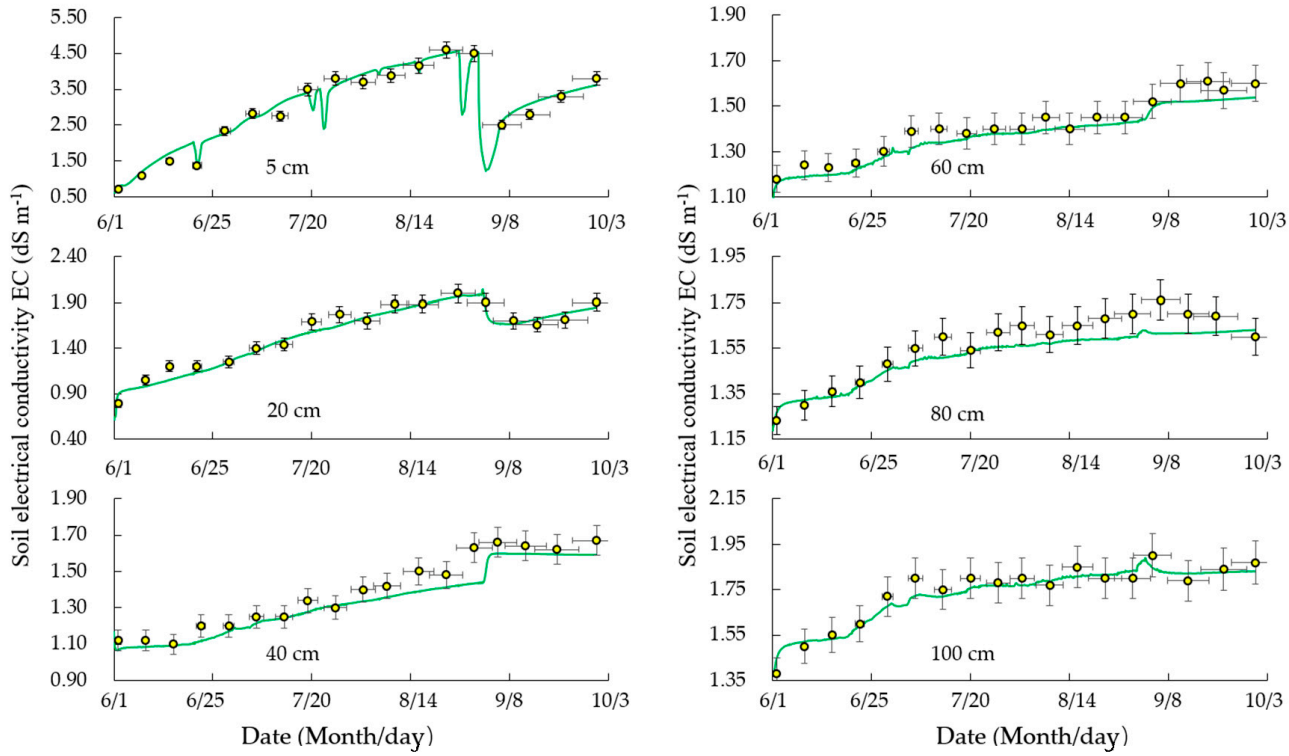

(**b**)

Figure 8. Model simulations (−) versus observed (·) soil water content (**a**) and soil electrical conductivity (**b**) for different layers of soil during the calibration of the model for the lake boundary.

Table 6. Values assigned to parameters to calculate the response to salt and water stress.

Equation	Parameter (cm)	Description	Sunflower Starting Values (cm)	Sunflower Calibration Values (cm)
Water Stress [35]	h_1	Absence of water extracted at elevated pressure heads	−0.1	−0.1
	h_2	h below that at which optimal water initiates	−10	−15
	h_{3h}	h below that at which a reduction in water uptake initiates at elevated atmospheric demand	−800	−400
	h_{3l}	h below that at which a reduction in water uptake initiates at low atmospheric demand	−1000	−700
	h_4	h below that at which there is zero water uptake	−10,000	−10,000
	$r2H$	Threshold of high atmospheric demand/(cm d^{-1})	0.5	0.5
	$r2L$	Threshold of low atmospheric demand/(cm d^{-1})	0.1	0.1
Salt Stress [37]	h^*_ϕ	Threshold of h_ϕ	−2800	−3600
	$h_{\phi 50}$	h_ϕ at which there is a reduction in the uptake of water by 50%	−6000	−8500

Note: h_ϕ represents the soil solution osmotic head and h represents the pressure head (cm).

3.2. Model Verification

The model was verified against experimental data from 2019. All model statistical coefficients and input parameters were carried over from the calibrated model. The verification results are shown in Figure 9. The soil water indicators (MRE, −0.92–0.63%; RMSE, 0.01–0.04 cm^3 cm^{-3}; R^2, 0.90–0.92; b, 0.98–1.01) and soil EC (MRE, −0.89–4.43%; RMSE, 0.15–0.34 dS m^{-1}; R^2, 0.56–0.89; b, 0.98–1.02) are shown in Table 6. The model verification results were acceptable.

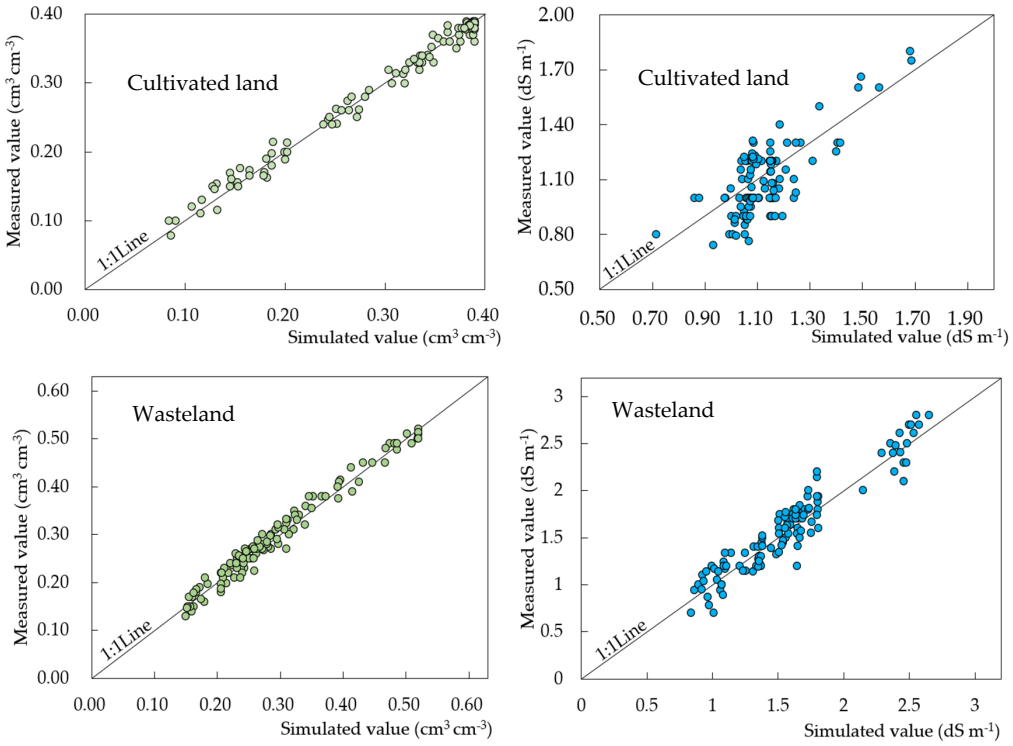

Figure 9. *Cont.*

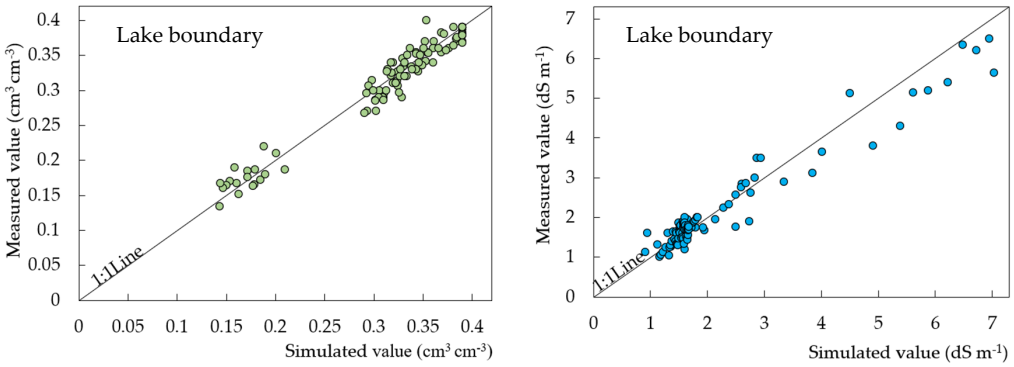

Figure 9. A comparison between observed and model-simulated soil water content (**left**) and soil electrical conductivity (**right**) for model verification for different land use types.

3.3. Soil Salt–Water Dynamics

3.3.1. Quantitative Estimation of the Moisture of Soil in a Typical Period

Since the climate did not significantly change from 2018 to 2019, the results for 2018 will be discussed below. The study area was irrigated on 23 June and 5 July. This study selected 22 June, 28 June, 4 July, 10 July, and 30 September as the typical dates to study characteristics of the salt and water transport in the 1 m soil zone of the cultivated land, wasteland, and lake boundary. The dynamics of the soil water are shown in Figure 10.

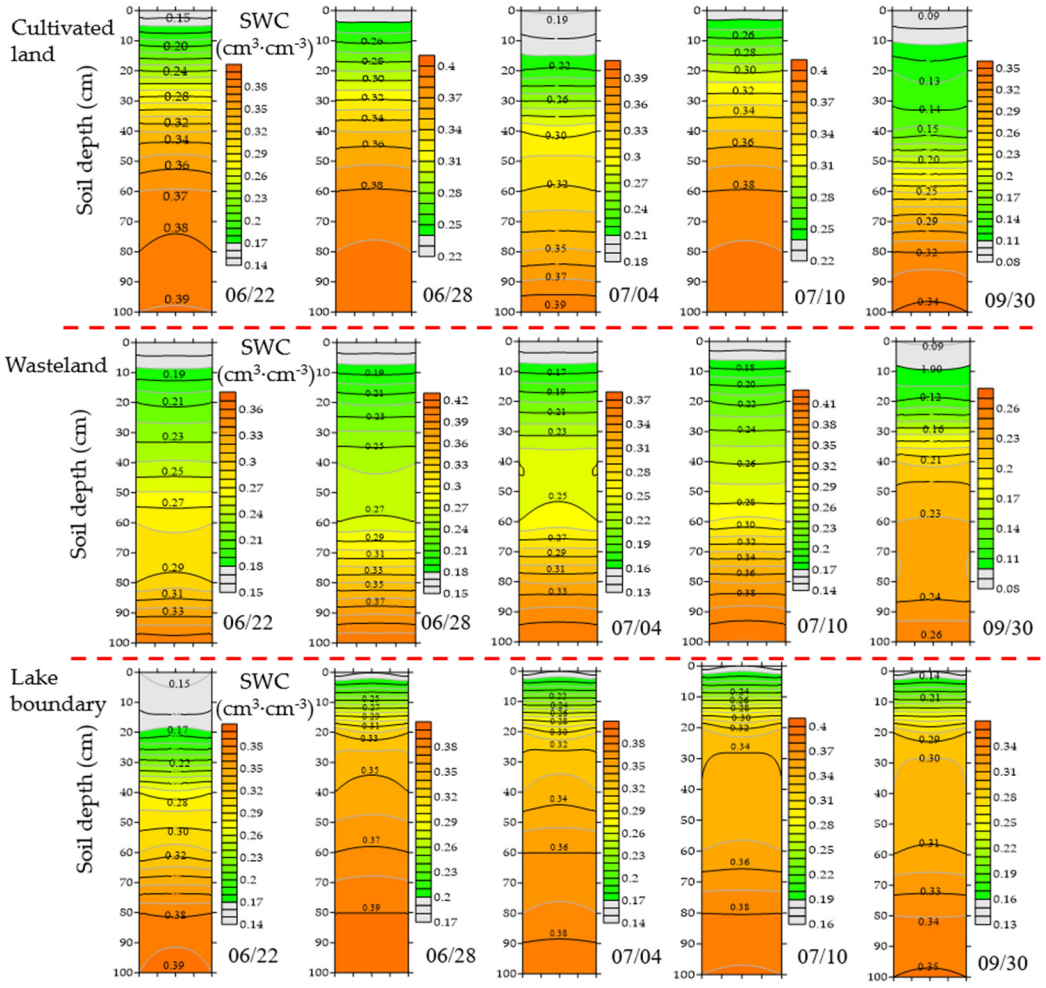

Figure 10. Changes of soil water content (SWC) in the cultivated land, wasteland, and lake boundary during different periods (from left to right: 22 June, 28 June, 4 July, 10 July, 30 September).

For the cultivated land, before and after the first irrigation (22 June–28 June), the soil water in the 0–20 cm soil zone changed greatly; i.e., it increased by 41%, and the water of the 20–60 cm soil zone increased by 18–20%, while changes in water in the 60–100 cm soil zone were not obvious. The first irrigation was 104 mm, and the water storage in the 1 m soil zone increased by 81 mm on the fifth day after irrigation; therefore, the utilization efficiency of irrigation was 78%. On the 11th day after irrigation (11 July), the soil water storage decreased by 66 mm compared with that on 28 June, when water in the 0–20 cm soil layer declined by 27%; for the 20–60 cm layer, it declined by 14–16%, and the change in the 80–100 cm layer was not obvious. Before and after the second irrigation (4 July–10 July), the water storage in the 1 m soil zone increased by 69 mm because the water in the second irrigation was 96 mm, and the utilization coefficient of the irrigation water was 72%, which was 6% less than that of the first irrigation. The interval between the first and the second irrigation was short. After the second irrigation, the changes in the soil water storage were smaller. The water in the 0–20 cm soil zone increased by 27%; in the 20–60 cm soil zone, it increased by 14–16%; and the change was not visible in the 80–100 cm layer. On the 87th day (30 September) after irrigation, soil water storage decreased by 186 mm. Soil water in the 0–20 cm soil zone declined by 56%; in the 20–40 cm soil zone, it declined by 57%; in the 40–60 cm soil zone, it declined by 34%; and in the 60–100 cm soil zone, it declined by 13–18%.

For the wasteland, the storage of water in the 1 m layer of soil increased by 36 mm (22 June–28 June), while soil water in the 60–80 cm soil zone increased by 15%; in the 80–100 cm layer, it increased by 12%, while soil water changes in the 0–40 cm layer were not obvious. After irrigation, the groundwater level of the wasteland rose, which caused the water in the deep soil zone to increase. Water storage in the 1 m soil zone increased by 51 mm from 4 July to 10 July, which was 15 mm higher than that of the first irrigation. After the second irrigation, the groundwater level of the wasteland rose more than that of the first irrigation (Figure 4). Water in the 40–100 cm layer increased by 12–14%, and in the upper soil zone, it showed a slightly increasing trend. Soil water storage decreased by 150 mm from 10 July to 30 September, when water in the 0–20, 20–60, and 60–100 cm soil zones decreased by 45%, 20%, and 37%, respectively.

For the lake boundary, the storage of water in the 1 m soil zone increased by 27 mm (22 June–28 June). Owing to shallow groundwater depth, water in the 60–100 cm layer was close to saturation, and water in the 0–60 cm soil zone increased by 6–9%. Water storage in the 1 m soil zone increased by 9 mm (4 July–10 July). Since the interval between the first and the second irrigation was short, soil water in the deep soil zone was saturated, and water in the 0–40 cm soil zone increased by 3–6%. The water storage in the 1 m soil zone decreased by 60 mm (10 July–30 September).

3.3.2. Quantitative Estimation of Soil Salt in a Typical Period

The dynamics of soil EC are shown in Figure 11. For cultivated land, soil salt in the 0–20 cm soil zone decreased by 26% (22 June–28 June), while in the 80–100 cm soil zone, it increased by 24%. Soil salt in the 0–20 cm soil zone decreased by 20% (4 July–11 July), while in the 80–100 cm soil zone, it increased by 9%. Since the interval between the first and the second irrigation was only 12 days, the amount of accumulated salt in the soil profile was very small. The leached salt from the upper soil zone after the second irrigation was 6% less than that after the first irrigation, while the salt in the deep soil zone increased by 15%. The salt in the 0–20 cm soil zone increased by 49% (10 July–30 September). The salt in the 0–20 cm soil zone increased by 13% (22 June–30 September), which shows a slightly increasing trend, and in the 20–40 cm and 40–60 cm soil zones, it increased by 5% and 26%, respectively.

For the wasteland, soil salt in the 0–10 cm soil zone on 22 June–June 28 and 4 July–10 July increased by 20% and 6%, respectively. After the first irrigation, the salt accumulation in the upper soil zone was 14% larger than that after the second irrigation. After the first irrigation, a large amount of groundwater salt in the cultivated land was transported to

the wasteland groundwater, which caused the salt in the deep soil zone to increase (80 cm, 1.09–1.20 dS/m; 100 cm, 1.09–1.20 dS m^{-1}). The salt in the upper soil zone increased by 15%, and in the deep soil zone, it increased by 11% from 10 July to 30 September. The salt in the upper soil zone increased by 37%, and in the deep soil zone, it increased by 15% from 22 June to 30 September. Owing to strong evaporation, the accumulated salt content in the upper soil zone was high.

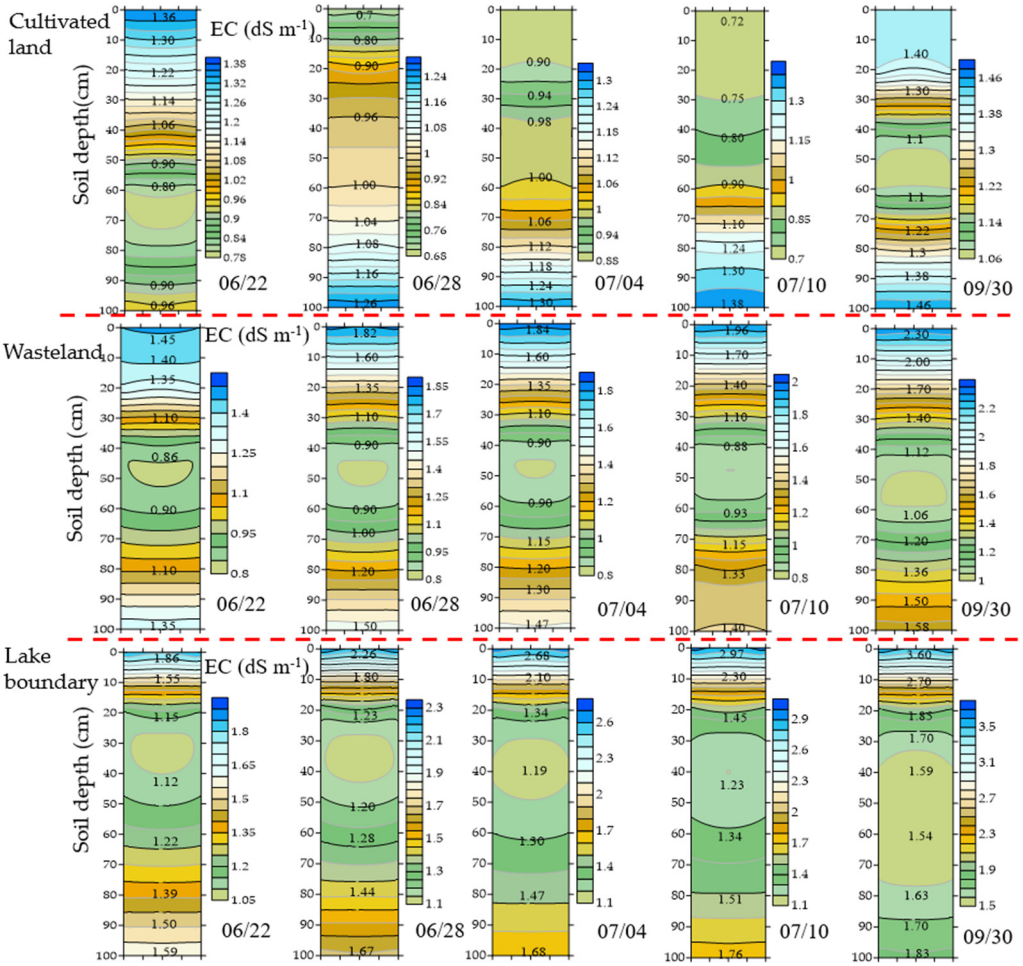

Figure 11. Changes in soil electrical conductivity (EC) in the cultivated land, wasteland, and lake boundary in the different periods (from left to right: 22 June, 28 June, 4 July, 10 July, 30 September).

For the lake boundary, the salt in the upper soil zone increased by 48%, and in the deep soil zone, it increased by 13%. The amount of accumulated salt in the upper soil zone was 35% greater than in the deep soil zone from 22 June to 30 September. During the irrigation period, the groundwater salt in the wasteland was transported to the lakes, which caused salt accumulation in the deep soil zone (80–100 cm). Those factors, including shallow groundwater depth, sandy loam in the 0–20 cm soil zone, and sand in the 20–100 cm soil zone, are beneficial to salt accumulated in the upper soil zone.

3.4. Soil Salt and Water Balance Analysis

As shown in Table 7, there were significant differences in the water–salt balance in the 0–100 cm soil zone of the cultivated land (A), wasteland (B), and lake boundary (C). During the growth period in 2018 and 2019, the irrigation water was 200 mm and 210 mm, respectively. The cultivated land was mainly affected by irrigation, while the wasteland and the lake boundary were not. Therefore, the deep percolation and capillary rise in the cultivated land, wasteland, and lake boundary in the study area were quite differ-

ent. During the growth period in 2018 and 2019, the deep percolation of the cultivated land was 105 mm and 110 mm, which was 34% and 40% of the applied water (rainfall and irrigation), respectively. The capillary rise in the cultivated land was 118 mm and 140 mm, which was 24% of the evapotranspiration. The capillary rises in the wasteland was 29% and 35% of their own evaporation, and those of the lake boundary were 62% and 68% of their own evaporation in 2018–2019, respectively. The salt storage in the 1 m soil zone of the cultivated land, wasteland, and lake boundary had an increasing trend, which was an average increase of 19%, 27%, and 37%, respectively. Under the effects of irrigation and rainfall on cultivated land, the amount of salt for percolation and capillary rise varied greatly from 2012 to 1568 g m^{-2} and from 2291 to 1904 g m^{-2} from 2018 to 2019, respectively. The capillary rise salt in the wasteland and the lake boundary was an average of 2519 and 7331 g m^{-2} from 2018 to 2019, respectively. Owing to the shallow groundwater depth and the high groundwater TDS in the lake boundary, the capillary rise salt in the lake boundary was three times that of the wasteland.

Table 7. Salt and water balance in the 0–100 cm soil profile during the simulation period from June 1st to October 1st in 2018 and 2019.

Year	Site	Soil Water /Salt	Precipitation	Irrigation	Initial Storage	Final Storage	Percolation	Capillary Rise	Evaporation	Transpiration
2018	A	Soil water (mm)	109.6	200	540	374	105	118	166	324
		Salt (g m^{-2})	—	120	7743	10,007	2012	2291	—	—
	B	Soil water (mm)	109.6	—	586	383	20	123	423	—
		Salt (g m^{-2})	—	—	7935	11,172	460	2336	—	—
	C	Soil water (mm)	109.6	—	610	530	21	271	440	—
		Salt (g m^{-2})	—	—	9970	15,553	622	7370	—	—
2019	A	Soil water (mm)	64.88	210	583	306	110	140	202	380
		Salt (g m^{-2})	—	126	7222	8459	1568	1904	—	—
	B	Soil water (mm)	64.88	—	655	394	50	151	432	—
		Salt (g m^{-2})	—	—	9420	12,666	934	2702	—	—
	C	Soil water (mm)	64.88	—	649	531	47	289	425	—
		Salt (g m^{-2})	—	—	11,318	18,196	1228	7291	—	—

4. Discussion

4.1. The Effects of Irrigation, Groundwater Dynamics, and Soil Texture on Soil Water and Salt Distribution

In recent years, with the implementation of water-conservation projects, the salt and water balance system that had been formed over many years has been disrupted. On the basis of the Hydrus-1D model, a soil water–salt transport analysis and a balance analysis in a cultivated land–wasteland–lake system were performed.

This study found that the groundwater table and soil water content in the deep soil zone of the wasteland and lake boundary rose during the irrigation period, and soil water content in the 60–100 cm soil zone of the wasteland increased by 12–15%. Li et al. (2010) showed that groundwater lateral flow between the cultivated land and wasteland was engendered after irrigation, and they also found that soil water content in the 20–70 cm soil zone of the wasteland increased by 4–11% [17]. Our result was larger than that of Li because it is difficult to increase water in the 20–40 cm soil zone with capillary action. This study found that the utilization efficiency of irrigation was 78%. Wang et al. (2020), based on the δD and $\delta^{18}O$ isotopes, revealed that the utilization efficiency of irrigation was 82% [41]. The results showed there was a sharp decline in soil EC with irrigation, after which it gradually increased prior to the subsequent irrigation. Hao et al. (2015) showed that irrigation water diluted the soil solution, and the salt was leached to the deep soil zone [42]. He et al. (2017) used the Hydrus-1D model to study the irrigated cropping system, and they showed that freshwater irrigation can leach out salts from the 100 cm root-profile depth [43]. Tong et al. (2018) found that the mean soil salt reduction rate under drip irrigation and sub-surface pipe drainage was 19.30% and 58.12%, respectively [44]. This study found that soil salt in the 0–20 cm soil zone of cultivated land decreased by 20~26% during the irrigation period. The salt reduction rate of the border irrigation was

higher than that of drip irrigation but lower than that of the sub-surface pipe drainage. This study found that the salt storage in the 1 m soil zone of the cultivated land, wasteland, and lake boundary had an increasing trend, which was an average increase of 19%, 27%, and 37%, respectively. Wang et al. (2021) studied the soil water and salt transport process in a sand dune–wasteland–lake system, and they found that the salt accumulation rate of the wasteland in the 1 m soil zone was 25% during the growth period [45]. Their study results are similar to ours, which indicates that the wasteland was in a state of salt accumulation during the growth period. During the growth period, the lake boundary was in a state of salt accumulation. Those factors, including shallow groundwater depth, sandy loam in the 0–20 cm soil zone, and sand in the 20–100 cm soil zone, are beneficial to the salt accumulated in the upper soil zone; conversely, those factors are not good for the upward movement of salt and water due to weak capillary action. Chen et al. (2010) found that it is significant and necessary for salinity control to conduct large flood irrigation to decrease salt accumulation after harvest [46].

4.2. Soil Water and Salt Balance Analysis

We revealed that the deep percolation of cultivated land was 34–40% of the applied water (rainfall and irrigation). Ren et al. (2018) pointed out that about 36% of the total applied water was stored in shallow groundwater [31], which indicated that the results of this study are acceptable. Ren et al. (2016) found that capillary rise in watermelon, sunflower, and maize fields accounted for over 45%, 24%, and 33% of their respective total evapotranspiration [5]. Xu et al. (2015) found that cumulative capillary rise could reach 40% of evapotranspiration when the groundwater depth was set to 100 cm [47]. We found that capillary rise in the cultivated land, wasteland, and lake boundary was 24%, 29–35%, and 62–68% of their own evapotranspiration, respectively. These results are similar to prior studies, which were credible. The capillary rise in the lake boundary was larger than that of the wasteland since the groundwater table of the lake boundary was 30 cm~140 cm during the growth period (Figures 3 and 4). Ren et al. (2019) pointed out that 40% of the total salt was retained in a wasteland, and 39% was retained in farmland [48]. Li et al. (2010) showed that the wasteland was in a state of salt accumulation, and salt accumulation in the upper soil zone was the most serious [17]. Based on the previous research, we further found that the salt accumulation in the upper soil zone of the cultivated land, wasteland, and lake boundary was 13%, 37%, and 48%, respectively, and in the deep soil zone, it was 34%, 15%, and 13%, respectively, which is significant in preventing soil salinization in the Hetao Irrigation District. This study suggests some measures should be taken to reduce the salt content in the upper soil zone of the wasteland and lake boundary and in the deep soil zone of the cultivated land to prevent soil salinization.

5. Conclusions

The Hydrus-1D model was successfully used to evaluate the soil salt and water transport characteristics of the cultivated land, wasteland, and lake boundary in the HID. The simulations of the model provide a good representation of measurements. The conclusions are as follows:

(1) On the fifth day after irrigation, the soil water storage increments of the cultivated land, wasteland, and lake boundary were 69~81 mm, 36~51 mm, and 9~22 mm, respectively; in particular, the soil water content in the 60–100 cm soil zone of the wasteland increased by 12–15%. On the 87th day after irrigation, the water storage in the cultivated land, wasteland, and lake boundary decreased by 186 mm, 150 mm, and 60 mm; the soil water content in the 0–60 cm soil zone of the cultivated land and wasteland decreased by 34–56% and 20–45%.

(2) The deep percolation of cultivated land was 34–40% of the applied water (rainfall and irrigation). The capillary rise in the cultivated land, wasteland, and lake boundary was 24%, 29–35%, and 62–68% of their own evapotranspiration, respectively.

(3) In the whole growth period, the salt storage in the 1 m soil zone of the cultivated land, wasteland, and lake boundary, on average, increased by 19%, 27%, and 37%, respec-

tively. Salt accumulation in the upper soil zone of the cultivated land, wasteland, and lake boundary was 13%, 37%, and 48%. Soil salinization in the upper soil zone of the wasteland and lake boundary was serious, so some measures should be taken to reduce the salt content to prevent soil salinization.

(4) Since the study scale of the cultivated land, wasteland, and lake systems was small, the simulation accuracy of the regional hydrological model is limited. It is necessary to expand the study area and establish a large hydrological monitoring network to study the hydrological process in the future.

Author Contributions: G.W. and H.S. conceived and designed the experiments. G.W. developed the initial and final versions of this manuscript and analyzed the data. B.X. and P.T. contributed their expertise and advice. D.T., Z.L. and J.R. conducted the experiments. C.Z. supported the writing of the manuscript. All authors have read and agreed to the published version of the manuscript.

Funding: This study was funded by Inner Mongolia National Natural Science Foundation, No. 2022QN05027, and the Key Project of National Natural Science Foundation, No. 51539005.

Informed Consent Statement: Written informed consent has been obtained from the patient(s) to publish this paper.

Acknowledgments: Authors acknowledge the support from Inner Mongolia National Natural Science Foundation, No. 2022QN05027, and the Key Project of National Natural Science Foundation, No. 51539005.

Conflicts of Interest: The authors declare no conflict of interest.

References

1. Xue, J.; Huo, Z.; Shuai, W.S. A novel regional irrigation water productivity model coupling irrigation- and drainage-driven soil hydrology and salinity dynamics and shallow groundwater movement in arid regions in China. *Hydrol. Earth Syst. Sci.* **2020**, *24*, 2399–2418. [CrossRef]
2. Chang, X.; Gao, Z.; Wang, S.; Chen, H. Modelling long-term soil salinity dynamics using Saltmod in Hetao irrigation district, china. *Comput. Electron. Agric.* **2019**, *156*, 447–458. [CrossRef]
3. Luo, Y.; Sophocleous, M. Seasonal groundwater contribution to crop-water use assessed with lysimeter observations and model simulations. *J. Hydrol.* **2010**, *389*, 325–335. [CrossRef]
4. Karimov, A.K.; Šimůnek, J.; Hanjra, M.A.; Avliyakulov, M.; Forkutsa, I. Effects of the shallow water table on water use of winter wheat and ecosystem health: Implications for unlocking the potential of groundwater in the Fergana Valley (Central Asia). *Agric. Water Manag.* **2014**, *131*, 57–69. [CrossRef]
5. Ren, D.; Xu, X.; Hao, Y.; Huang, G. Modeling and assessing field irrigation water use in a canal system of Hetao, upper Yellow River basin: Application to maize, sunflower and watermelon. *J. Hydrol.* **2016**, *532*, 122–139. [CrossRef]
6. Wang, X.Z.; Gao, Q.Z.; Lu, Q. Effective use of water resources, and salinity and waterlogging control in the Hetao Irrigation Area of Inner Mongolia. *J. Arid Land Res. Environ.* **2005**, *19*, 118–123. (In Chinese with English abstract)
7. Wang, Y.D. Analysis on changes of groundwater table before and after water saving reconstruction in Hetao Irrigation District. *Water Sav. Irrig.* **2002**, *1*, 15–17. (In Chinese with English abstract)
8. Dou, X.; Shi, H.; Li, R.; Miao, Q.; Tian, F.; Yu, D.; Zhou, L.; Wang, B. Effects of Controlled Drainage on the Content Change and Migration of Moisture, Nutrients, and Salts in Soil and the Yield of Oilseed Sunflower in the Hetao Irrigation District. *Sustainability* **2021**, *13*, 9835. [CrossRef]
9. Wang, G.S.; Shi, H.B.; Li, X.Y.; Guo, J.; Wang, W.; Wu, D. Estimation of salt transport and relationship with groundwater depth in different land types in Hetao Irrigation Area. *Trans. CSAM* **2020**, *51*, 255–269. (In Chinese with English abstract)
10. Han, L.; Liu, D.; Cheng, G.; Zhang, G.; Wang, L. Spatial distribution and genesis of salt on the saline playa at Gehan lake, inner Mongolia, China. *Catena* **2019**, *177*, 22–30. [CrossRef]
11. Wu, J.; Zhao, L.; Huang, J.; Yang, J.; Vincent, B.; Bouarfa, S.; Vidal, A. On the effectiveness of dry drainage in soil salinity control. *Sci. China Ser. E* **2009**, *52*, 3328–3334. [CrossRef]
12. Qi, Z.; Feng, H.; Zhao, Y.; Zhang, T.; Zhang, Z. Spatial distribution and simulation of soil moisture and salinity under mulched drip irrigation combined with tillage in an arid saline irrigation district, northwest China. *Agric. Water Manag.* **2018**, *201*, 219–231. [CrossRef]
13. Zhu, Y.; Shi, L.S.; Yang, J.Z. Coupling methodology and application of a fully integrated model for contaminant transport in the subsurface system. *J. Hydrol.* **2013**, *501*, 56–72. [CrossRef]
14. Mao, W.; Yang, J.Z.; Zhu, Y. Loosely coupled SaltMod for simulating groundwater and salt dynamics under well-canal conjunctive irrigation in semi-arid areas. *Agric. Water Manag.* **2017**, *192*, 209–220. [CrossRef]

15. Xu, X.; Huang, G.H.; Zhan, H.B.; Qu, Z.; Huang, Q. Integration of SWAP and MODFLOW-2000 for modeling groundwater dynamics in shallow water table areas. *J. Hydrol.* **2012**, *412*, 170–181. [CrossRef]
16. Ren, D.; Wei, B.; Xu, X. Analyzing spatiotemporal characteristics of soil salinity in arid irrigated agro-ecosystems using integrated approaches. *Geoderma* **2019**, *356*, 113935. [CrossRef]
17. Li, L.; Shi, H.B.; Jia, J.F. Simulation of water and salt transport of uncultivated land in Hetao Irrigation District in Inner Mongolia. *Trans. CSAE* **2010**, *26*, 31–35. (In Chinese with English abstract)
18. Kanzari, S.; Ben Nouna, B.; Mariem, S.B.; Rezig, M. Hydrus-1d model calibration and validation in various field conditions for simulating water flow and salts transport in a semi-arid region of Tunisia. *Sustain. Environ. Res.* **2018**, *28*, 350–356. [CrossRef]
19. Bashir, R.; Chevez, E.P. Spatial and seasonal variations of water and salt movement in the vadose zone at salt-impacted sites. *Water* **2018**, *10*, 1833. [CrossRef]
20. Dong, W.; Wen, C.; Zhang, P.; Su, X.; Yang, F. Soil water and salt transport and its influence on groundwater quality: A case study in the Kongque river region of China. *Pol. J. Environ. Stud.* **2018**, *28*, 1637–1650. [CrossRef]
21. Wu, X.; Xia, J.; Zhan, C.; Jia, R.; Zou, L. Modeling soil salinization at the downstream of a lowland reservoir. *Hydrol. Res.* **2019**, *50*, 1202–1215. [CrossRef]
22. Slama, F.; Gargouri-Ellouze, E.; Bouhlila, R. Impact of rainfall structure and climate change on soil and groundwater salinization. *Clim. Chang.* **2020**, *163*, 395–413. [CrossRef]
23. Liu, B.; Wang, S.; Kong, X.; Liu, X.; Sun, H. Modeling and assessing feasibility of long-term brackish water irrigation in vertically homogeneous and heterogeneous cultivated lowland in the north china plain. *Agric. Water Manag.* **2019**, *211*, 98–110. [CrossRef]
24. Wang, X.; Gao, Q.; Lu, Q.; Li, B. Salt-water Balance and Dry Drainage Desalting in Hetao Irrigating Area. Inner Mongolia. *Sci. Geogr. Sin.* **2006**, *26*, 455–460. (In Chinese with English abstract)
25. Xu, X.; Huang, G.; Qu, Z.; Pereira, L.S. Assessing the groundwater dynamics and impacts of water saving in the Hetao irrigation district, yellow river basin. *Agric. Water Manag.* **2010**, *98*, 301–313. [CrossRef]
26. Wu, J.W.; Vincent, B.; Yang, J.Z.; Bouarfa, S.; Vidal, A. Remote sensing monitoring of changes in soil salinity: A case study in Inner Mongolia, China. *Sensors* **2008**, *8*, 7035–7049. [CrossRef]
27. Allen, R.G.; Pereira, L.S.; Raes, D.; Smith, M. *Crop Evapotranspiration, Guidelines for Computing Crop Water Requirements*; FAO Irrigation and Drainage Paper 56; FAO-Food and Agriculture Organisation of the United Nations: Rome, Italy, 1998.
28. Shi, H.B.; Guo, J.W.; Zhou, H. Effects of irrigation amounts and groundwater regulation on soil water and salt distribution in Arid Region. *Trans. CSAM* **2020**, *51*, 268–278, (In Chinese with English Abstract).
29. Tong, W.J. Study on salt tolerance of crops and cropping system optimization in Hetao Irrigation District. Ph.D. Thesis, China Agricultural University, Beijing, China, 2014. (In Chinese).
30. Xu, X.; Huang, G.H.; Chen, S. Assessing the effects of water table depth on water use, soil salinity and wheat yield: Searching for a target depth for irrigated areas in the upper Yellow River basin. *Agric. Water Manag.* **2013**, *125*, 46–60. [CrossRef]
31. Ren, D.Y.; Xu, X.; Huang, G.H.; Huo, Z.; Xiong, Y.; Huang, G. Analyzing the role of shallow groundwater systems in the water use of different land-use types in arid irrigated regions. *Water* **2018**, *10*, 634. [CrossRef]
32. Šimunek, J.; Šejna, M.; Saito, H.; Sakai, M.; van Genuchten, M.T. *The HYDRUS-1D Software Package for Simulating the Movement of Water, Heat, and Multiple Solutes in Variably-Saturated Media*; Version 4.08; HYDRUS Software Series 3; University of California Riverside: Riverside, CA, USA, 2009; p. 315.
33. van Genuchten, M.T. A closed form equation for predicting the hydraulic conductivity of unsaturated soils. *Soil Sci. Soc. Am. J.* **1980**, *44*, 892–898. [CrossRef]
34. Mualem, Y. A new model for predicting hydraulic conductivity of unsaturated porous media. *Water Resour. Res.* **1976**, *12*, 513–522. [CrossRef]
35. Fedds, R.A.; Kowalik, P.J.; Zaradny, H. *Simulation of Field Water Use and Crop Yield*; John Wiley and Sons: New York, NY, USA, 1978.
36. van Genuchten, M.T.; Hoffman, G.J. *Analysis of Crop Salt Tolerance Data*; Shainberg, I., Shalhevet, J., Eds.; Soil Salinity under Irrigation: Processes and Management; Springer: Berlin/Heidelberg, Germany,, 1984; pp. 258–271.
37. Dirksen, C.; Augustijn, D.C. Root water uptake function for nonuniform pressure and osmotic potentials. In *Agronomy Abstract ASA*; Springer: Madison, WI, USA, 1988; p. 185.
38. Homaee, M.; Dirksen, C.; Feddes, R.A. Simulation of root water uptake: I. Nonuniform transient salinity using different macroscopic reduction functions. *Agric. Water Manag.* **2002**, *57*, 89–109. [CrossRef]
39. Goudriaan, J. *Crop Micrometeorology: A Simulation Study*; Wageningen University and Research: Wageningen, The Netherlands, 1977.
40. Belmans, C.; Wesseling, J.G.; Feddes, R.A. Simulation model of the water balance of a cropped soil: SWATRE. *J. Hydrol.* **1983**, *63*, 271–286. [CrossRef]
41. Wang, G.; Shi, H.; Li, X.; Yan, J.; Guo, J.; Li, Z. Study on migration of different types water during farmland-wasteland-lake system in Hetao Irrigation District. *Adv. Water Sci.* **2020**, *31*, 832–842.
42. Hao, Y.Y.; Xu, X.; Ren, D.Y.; Huang, Q.; Huang, G. Distributed modeling of soil water-salt dynamics and crop yields based on HYDRUS-EPIC model in Hetao Irrigation District. *Trans. CSAE* **2015**, *31*, 110–116. (In Chinese with English abstract)
43. He, K.; Yang, Y.; Yang, Y.; Chen, S.; Hu, Q.; Liu, X.; Gao, F. HYDRUS Simulation of Sustainable Brackish Water Irrigation in a Winter Wheat-Summer Maize Rotation System in the North China Plain Water. *Water* **2017**, *9*, 536. [CrossRef]
44. Tong, H.; Liao, R.; Wang, Z.; Wu, W.; Li, W.; Zhang, J. Effects of combined drip irrigation and sub-surface pipe drainage on water and salt transport of saline-alkali soil in Xinjiang, China. *J. Arid Land* **2018**, *10*, 932–945.

45. Wang, G.; Shi, H.; Li, X. Simulation and evaluation of soil water and salt transport in desert oases of Hetao Irrigation District using HYDRUS-1D model. *Trans. CSAE* **2021**, *37*, 87–98. (In Chinese with English abstract)
46. Chen, W.; Hou, Z.; Wu, L.; Liang, Y.; Wei, C. Evaluating salinity distribution in soil irrigated with saline water in arid regions of northwest China. *Agric. Water Manag.* **2010**, *97*, 2001–2008. [CrossRef]
47. Xu, X.; Sun, C.; Qu, Z.Y.; Huang, Q.Z.; Ramos, T.B.; Huang, G.H. Groundwater recharge and capillary rise in irrigated areas of the upper yellow river basin assessed by an agro-hydrological model. *Irrig. Drain* **2015**, *64*, 587–599. [CrossRef]
48. Ren, D.Y.; Xu, X.; Huang, G.H. Irrigation water use in typical irrigation and drainage system of Hetao Irrigation District. *Trans. CSAE* **2019**, *35*, 98–105. (In Chinese with English abstract)